



Defect Characterization in a 1D Spring Mass System Using the Laplace and Z-Transforms

Neil Jerome A. Egarguin¹ · Larry Guan² · Daniel Onofrei²

Received: 16 June 2021 / Revised: 17 January 2022 / Accepted: 18 January 2022
© Krishtel eMaging Solutions Private Limited 2022

Abstract

Purpose We present a scheme to characterize the defects within a one-dimensional spring–mass system comprised of an arbitrary number of bodies with otherwise uniform masses connected in series by springs using only a discrete set of vibrational data of the first body.

Methods The system of ordinary differential equations modeling spring–mass systems was analyzed using the Laplace transform with the unknown mass and location of the defects as parameters. We propose a two-phase strategy to determine these unknown parameters using a set of discrete measurements of the longitudinal displacements of the first mass after the system is excited by a Dirac δ impulse on the first mass. The Z-transform of the discrete time-measurements is used to obtain an approximation for the Laplace-domain solution curve of the vibration of the first body. First, we show how the poles of this simulated data can be used to determine the masses of the defects. Then the location of these defects were calculated using an optimization routine.

Results We also show several simulations with two defects highlighting the instances when the scheme is highly accurate as well as its limitations. In these cases, the algorithm was able to predict the mass and locations accurately.

Conclusions In this paper, we were able to design a stable numerical scheme that can characterize the defects, i.e., estimate their masses and locations, using only a discrete set of vibrational data of the first mass.

Keywords Defect detection · Spring–mass system · Laplace transform · Z-transform

Introduction

Spring–mass systems are extensively used models across a multitude of disciplines ranging from medicine, computer animation and engineering. The primary advantages of this model include (but are not limited to) its simple intuitive description, relative mathematical simplicity and ease of computational implementation. Due to the prevalence of spring–mass models across these disciplines, it is hard to conduct a comprehensive literature survey. Consequently, a brief overview consisting of select illustrations will be presented.

Within the medical field, the spring–mass model can be used to simulate the deformational properties of human organs [15, 23, 34]. The parameters needed to calibrate the spring–mass array to be accurate models of real organs could be determined through methods employed in Ref. [33] and appropriately configured for virtual surgeon training [28]. It is also possible to analyze the mechanics of human or bipedal locomotion relating to walking [17], running [19], and Olympic sprinting [29] using spring–mass models.

Animators seeking high-fidelity fabric dynamics will find utility in spring–mass models. While models derived from continuum mechanics are more physically consistent, it may be more practical to trade off high-accuracy methods for quicker simulations due to the discrete nature of spring–mass arrays. The works [18, 31, 35] provide deeper discussions on this application. Use of spring–mass systems in other fields of computer graphics and animations can be found in the review article [22].

Further afield, some mechanical engineering disciplines focus on studying how to suppress vibrations within a structure

✉ Neil Jerome A. Egarguin
naegarguin1@up.edu.ph

¹ Institute of Mathematical Sciences and Physics, University of the Philippines Los Baños, Los Baños, Laguna, Philippines

² Department of Mathematics, University of Houston, Houston, TX, USA

[2, 10, 26] or a metamaterial [13] or combining the two to suppress structural vibrations using metamaterials [25]. Vibration suppression is also an integral part of vehicular suspension systems. Spring–mass systems are used as computational models to design improvements to semi-adaptive (or fully adaptive) suspension systems which can improve the comfort and safety of passengers inside moving vehicles [27, 30].

One dimensional spring–mass systems, despite its simplicity, prove to be very useful models in acoustics, electromagnetism (EM) and atomic lattices and other periodic materials. In acoustics, they can be realized as discrete models for the propagation of sound in a duct and other environments [21]. These models can also be used for advanced applications such as in [32] where the authors realized cloaking in acoustic metamaterials. In EM, these systems are often used as mechanical analogies to electric circuits. This led to advances such as the characterization of the properties of the oscillations in electrical circuits [12], description of the transient behavior of driven RLC circuits [11] and the design of novel strategies for the active control of vibrations using piezoelectric materials and other related actuator-damper systems (see works like [4, 5] and references therein). In the field of periodic materials and atomic lattices, 1D spring–mass systems are used to simulate the wave propagation in phononic structures [6] and other crystalline lattices [20]. For a more generic discussion of the utility of springs and masses as computational models in lattice dynamics, see the review article [7].

Due to the wide physical applications of spring–mass systems, it is worthwhile to design schemes to detect and characterize defects as these can profoundly alter a system's reaction to external forces. For instance, defects within photonic crystals or dielectric media can act as waveguides for incident light [16]. In another vein, regional deviations of mass density within a rod would change its mode shapes [1]. An example of defectoscopy via subjecting the system to some external excitation is found in [3]. In said paper, defects within polymers were identified by subjecting the material to an impulse and measuring changes in their resonant frequency. Defectoscopy on a ball bearing subject to external vibrations was conducted by another group detailed in [24]. In this paper, we will build on the results and ideas proposed in [9] to develop a new computational scheme in detecting and characterizing defects in one-dimensional spring–mass systems.

In Ref. [9], the authors proposed a scheme in characterizing the defects in a system, the number of whom is assumed to be known. Their method involves comparing the theoretical solution for the vibration of the first mass expressed as

a function of the unknown parameters of the defects against some data. This data may be simulated or measured, but in both cases must be expressed as a continuous function in the Laplace domain for a long enough interval. Such a data may be difficult to obtain from physical measurements. Moreover, the method presented in Ref. [9] worked well only in the case of two unknown information (i.e., the location and size of one defect or the locations of two defects with known masses or the masses of two defects with known locations) and required a very high level of numerical precision, something that is not feasible from the point of view of even the most sophisticated measurement devices. In this work, we address some of these difficulties by providing a way of utilizing discrete time-measurements of the vibrations of the first mass to characterize the defects.

Assuming a known number of defects, we propose a stable technique that will yield the mass and location of the defects present in the physical configuration of springs and masses based solely on discrete measurements of the longitudinal vibrations of the first body, i.e., the body at the left end of the system.

In Fig. 1, there are an arbitrary number of bodies linked in series by identical springs which have fixed damping coefficient and stiffness constant. All bodies have a mass of unity, except for the defects. While Fig. 1 shows only two defects, multiple defects with different masses may be present. Similarly, they can be located anywhere along the chain, except on the left and right ends. At time $t = 0$, a sharp, impulsive force directed rightward will be applied to the leftmost body. To keep our model as realistic as possible, we assume that the vibrations of this body, $x_1(t)$, will be measured at some discrete t values and transformed into the Laplace domain via the Z-transform. In the discussions below, we shall establish a way on how to use this simulated data to recover the parameters of the defects. The rest of this paper is organized as follows. In Sect. 2 we present the mathematical model for a 1D spring mass system with an arbitrary number of defects. In Sect. 3, we detail the defect detection and characterization strategy by establishing the mathematical relation between the poles of the Laplace-domain vibration of the first mass and the masses of the defects and laying-out an optimization routine to recover the defects' locations. In Sect. 4, we present some implementations of the proposed scheme highlighting the advantages and limitations of the method. Finally, we offer some concluding remarks in Sect. 5.

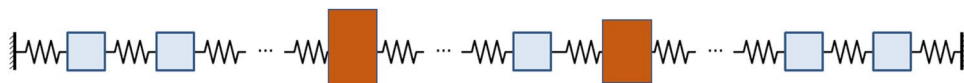


Fig. 1 The 1D spring–mass system of interest where the defective bodies are highlighted in red

Mathematical Model for the Spring–Mass System

This section discusses the mathematical model for a spring–mass system with defective bodies leading towards deriving the longitudinal trajectory of any body in the system after it has been excited by a Dirac delta force on one of the terminal masses. See Fig. 1. We assume a Hookean, linear spring–mass system consisting of some n bodies between two fixed, immobile points. Each body is particle-like with some mass and assigned a location number (an integer) L starting with 1 at the left end and increasing rightward along the chain up to n . All bodies has mass 1, except for p bodies with unknown mass $m_q \neq 1$ at unknown locations $j_q \geq 2, q = 1, p$. These bodies of non-unit mass are the defects and we wish to find their locations and masses.

The body at location 1 is excited at time $t = 0$ with a rightward Dirac delta force $\gamma\delta(t)$ (γ is a positive scalar denoting the amplitude of the testing force). In the absence of other external forces, the longitudinal displacement of each body from its respective equilibrium position x_L are given by the solution curves of the system of second-order ordinary differential equations (ODEs) with initial conditions seen as follows:

$$\begin{cases} \ddot{x}_1 + d\dot{x}_1 + 2kx_1 - kx_2 & = \gamma\delta(t) \\ \ddot{x}_2 + d\dot{x}_2 + 2kx_2 - kx_1 - kx_3 & = 0 \\ \vdots & \\ m_q\ddot{x}_{j_q} + d\dot{x}_{j_q} + 2kx_{j_q} - kx_{j_q-1} - kx_{j_q+1} & = 0, 1 \leq q \leq p \\ \vdots & \\ \ddot{x}_{n-1} + d\dot{x}_{n-1} + 2kx_{n-1} - kx_{n-2} - kx_n & = 0 \\ \ddot{x}_n + d\dot{x}_n + 2kx_n - kx_{n-1} & = 0 \\ x_L(0) = \dot{x}_L(0) = 0 & 1 \leq L \leq n \end{cases}, \tag{1}$$

where k is the spring constant and d is the damping coefficient of each spring. Both k and d are assumed invariant everywhere to model a homogeneous, isotropic material. System (1), of course, can be modified as needed to suit desired chain lengths and/or defect parameters.

The Laplace transform of system (1) is taken to obtain the matrix equation

$$\tilde{f} = (s^2\mathbf{I} + sdD_m - D_mA_e)\tilde{x}, \tag{2}$$

where

$$A_e = k \begin{pmatrix} -2 & 1 & & & & \\ 1 & -2 & 1 & & & \\ & 1 & -2 & 1 & & \\ & & \ddots & \ddots & \ddots & \\ & & & 1 & -2 & 1 \\ & & & & 1 & -2 \end{pmatrix} \tag{3}$$

and

$$D_m = \begin{pmatrix} 1 & & & & & \\ & 1 & & & & \\ & & \ddots & & & \\ & & & 1 & & \\ & & & & \frac{1}{m_1} & \\ & & & & & 1 \\ & & & & & & \ddots & \\ & & & & & & & \frac{1}{m_q} \\ & & & & & & & & \ddots & \\ & & & & & & & & & 1 \end{pmatrix}. \tag{4}$$

Specifically, $\tilde{x} = (\tilde{x}_1, \tilde{x}_2, \dots, \tilde{x}_n)^T$ is the column vector comprising of the Laplace transform of the functions describing the longitudinal displacement of each body in the system at time t , $\tilde{f} = (\gamma, 0, \dots, 0)^T$ is the post-transform forcing term, \mathbf{I} is the identity matrix of size $n \times n$, D_m is the diagonal matrix with entries corresponding to the reciprocal mass of each body down the chain and A_e is the coefficient matrix describing the springs acting on each body in the absence of damping.

Knowing the locations and masses of all defects, one can easily solve the forward problem (2) and obtain \tilde{x} . In [9], the simulated data \tilde{x}_1 representing the Laplace transform of the longitudinal vibration of mass 1 was used to recover the information about the defects. As mentioned above, this worked well only for the case of recovering two unknown defect parameters. Moreover, this sort of data, a continuous function in the Laplace domain might be difficult to obtain in a physical or experimental setting. In the succeeding sections, we discuss an alternative stable scheme in recovering the characteristics of the defects using discrete time measurements of the vibrations in the first mass.

Defect Detection Strategy

In this section, we will develop an algorithm to recover the masses and locations of the p defects present in the spring–mass system described in Sect. 2. First, discrete vibrational data is measured in the time domain and subjected to the Z-transform to obtain an approximation of the Laplace domain data \tilde{x}_1 . This process makes the scheme more feasible from a physical point of view as only discrete measurements are needed. It turns out, as we shall discuss below, that the poles of \tilde{x}_1 are related to the eigenvalues of the spring–mass system. These eigenvalues contain information regarding the defects’ masses that can be extracted using the invariants of the associated matrix (e.g., the trace and the determinant for the case of two defects). Then, knowing the masses, numerical minimization of an L^2 residual function will reveal the locations of each and every defect.

Obtaining the Input Data

As stated above, the proposed strategy uses some discrete measurements $\{x_1(t_i)|t_i = i\Delta t\}$ of the vibrations in the first mass over a time interval $[0, T]$ taken with a uniform time step Δt . This can be easily done in a laboratory with appropriate measurement devices. However, the strategy we propose requires some Laplace domain data. To obtain the Laplace domain data from the discrete time measurements, we apply the Z-transform as defined below.

Definition 3.1 Let X be a discrete time signal with a constant time step Δt . Its Z-transform \hat{X} is given by

$$\hat{X}(z) = \sum_{l=0}^{\infty} X(l\Delta t)z^{-l}. \quad (5)$$

In the presence of damping, the spring mass system will return to equilibrium after some sufficiently long period of time. Hence, for our purposes, the summation in (5) can be truncated as soon as negligible displacements are observed. Moreover, the Z-transform is closely related to the Laplace transform. In fact, letting $z = e^{s\Delta t}$ and for sufficiently small Δt , we have

$$\begin{aligned} \hat{X}(z)\Delta t &= \sum_{l=0}^{\infty} X(l\Delta t)e^{-ls\Delta t}\Delta t \\ &\approx \tilde{X}(s), \end{aligned} \quad (6)$$

where \tilde{X} is the Laplace transform of the continuous extension of the time signal X .

These properties allow us to obtain an approximation to a continuous Laplace domain data from discrete time measurements. At this point, one can apply the residual minimization approach proposed in Ref. [9] to obtain the characteristics of such defects. However, for a large number of defects, the dimension of the optimization problem becomes very large and an analytic solution extending the approach proposed in Ref. [9] developed extreme instabilities to noise (numerical or measurement noise). This also causes the numerical implementation of the previously proposed approach to be computationally extensive. In the succeeding sections, we discuss an alternative way of characterizing the defects which involves two steps: first, the determination the defects' masses using matrix invariants followed by the identification of their locations by minimizing some residual function. The first step involves solving a system of nonlinear equations while the second applies the same optimization procedure as in [9] but this time with a lesser number of unknowns.

Estimating the Eigenvalues of $D_m A_e$

In this subsection, we show that eigenvalues of the matrix $D_m A_e$, introduced at (2) and defined in (3), (4) can be well approximated using the poles of the input data \tilde{x}_1 (i.e., the Laplace transform of the time-domain displacement of the leftmost mass in the system). This is a key step in our strategy as these eigenvalues give (through Viète's relations for the characteristic polynomial of $D_m A_e$) the invariants of $D_m A_e$ involving the masses of the bodies in the system. These relations will be derived in the next section. Here we focus on establishing a way of estimating the eigenvalues of the said matrix using the input data we obtained from the procedure laid above.

We begin by establishing the diagonalizability of the matrix $D_m A_e$. Looking at the explicit forms given in (3) and (4), it is easy to surmise that D_m and A_e are both Hermitian. As such, we can assert the following result (excerpts of Corollary 7.6.2 in Ref. [14]).

Theorem 3.1 [14] *Let A and B be Hermitian $n \times n$ matrices.*

1. *If A is positive definite, then AB is diagonalizable and has real eigenvalues.*
2. *If A and B are positive semidefinite, then AB is diagonalizable and has nonnegative eigenvalues.*

Note that the matrix D_m is positive definite. Thus, the product $D_m A_e$ is diagonalizable. Moreover, A_e is negative definite, and so $-A_e$ is positive definite. These means $-D_m A_e$ has nonnegative eigenvalues or equivalently, $D_m A_e$ has nonpositive eigenvalues.

Since $D_m A_e$ is diagonalizable, there exists an $n \times n$ invertible matrix T such that:

$$D_m A_e = T\Lambda_m T^{-1}, \quad (7)$$

where Λ_m is the diagonal matrix with diagonal entries equal to the eigenvalues of $D_m A_e$. Returning to equation (2) and using (7), we obtain

$$\tilde{f} = (s^2\mathbf{I} + sdD_m - D_m A_e)\tilde{x} \quad (8)$$

$$s^2\tilde{x} = D_m A_e \tilde{x} - sdD_m \tilde{x} + \tilde{f} \quad (9)$$

$$= (T\Lambda_m T^{-1})\tilde{x} - sd(D_m T T^{-1})\tilde{x} + \tilde{f} \quad (10)$$

$$\implies s^2 T^{-1}\tilde{x} = \Lambda_m T^{-1}\tilde{x} - sdT^{-1}D_m T T^{-1}\tilde{x} + T^{-1}\tilde{f}. \quad (11)$$

Let $w = T^{-1}\tilde{x}$. This enables the previous Eq. (11) to be written as

$$s^2w = \Lambda_m w - sdT^{-1}D_mTw + T^{-1}\tilde{f} \tag{12}$$

$$\implies w = (s^2\mathbf{I} - \Lambda_m + sdT^{-1}D_mT)^{-1}T^{-1}\tilde{f} \tag{13}$$

$$= \frac{1}{s}(s\mathbf{I} - \frac{1}{s}\Lambda_m + dT^{-1}D_mT)^{-1}T^{-1}\tilde{f} \tag{14}$$

$$= \frac{1}{s}(A - B)^{-1}T^{-1}\tilde{f}, \tag{15}$$

where $A = s\mathbf{I} - \frac{1}{s}\Lambda_m$ and $B = -dT^{-1}D_mT$. Since the explicit form for T is unknown, we will assert a physical assumption that the damping coefficient is small, i.e., ($d \ll 1$) and use a Neumann series expansion. Provided that A^{-1} exists (which is always true whenever s^2 is not equal to an eigenvalue of Λ_m), we have

$$(A - B)^{-1} = [A(\mathbf{I} - A^{-1}B)]^{-1} = (\mathbf{I} - A^{-1}B)^{-1}A^{-1} \tag{16}$$

where

$$(\mathbf{I} - A^{-1}B)^{-1} = \sum_{\alpha=0}^{\infty} (A^{-1}B)^{\alpha} \tag{17}$$

$$= \mathbf{I} + A^{-1}B + (A^{-1}B)^2 + \dots \tag{18}$$

$$\approx \mathbf{I} + A^{-1}B, \tag{19}$$

for $d \ll 1$. Using this in Eq. (16) yields

$$(A - B)^{-1} \approx A^{-1} + A^{-1}BA^{-1}. \tag{20}$$

Since d is assumed to be small, the second term of the right-hand side of Eq. (20) can be ignored. The final result is obtained using this truncated approximation back into the original equation (15) for w :

$$w \approx \frac{1}{s}A^{-1}T^{-1}\tilde{f} \tag{21}$$

$$= (s^2\mathbf{I} - \Lambda_m)^{-1}T^{-1}\tilde{f}. \tag{22}$$

At this point, we note that an explicit expression for T is unnecessary for our purpose. Recall that $Tw = \tilde{x}$, and in particular, $\tilde{x}_1 = \sum_{l=1}^n T_{1l}w_l$. This means that at the poles of \tilde{x}_1 , the sum on the right-hand side must blow up. Equation (22) suggests that this occurs for $s^2 \approx \lambda$ for some eigenvalue λ of D_mA_e . There will be $2n$ poles on the complex

s -plane since they appear in conjugate pairs. Moreover, we know that the eigenvalues of D_mA_e are all non-positive, so the poles occur near the imaginary axis. Further, we only need to consider the poles present near the positive imaginary axis.

In summary, we have established a relationship between the eigenvalues of the system matrix D_mA_e and the poles of \tilde{x}_1 . Instead of an explicit symbolic expression for \tilde{x}_1 , we can use the approximation for it obtained via the Z-transform of the discrete-time data to get estimates for the eigenvalues of the system matrix. This will allow us to recover the masses of the defects, discussed next.

Recovering the Masses

After obtaining estimates for the eigenvalues, approximations to the mass of each defect can now be calculated. The following discussion proposes an explicit scheme of recovering the masses when there is one or two defects, though most of the analyses are still valid even for $p > 2$. For the case when $p = 2$, we shall use some relations involving the trace and determinant of the system matrix. Recall that the trace τ and determinant σ of D_mA_e are respectively the sum and product of its n eigenvalues. These two parameters can also be expressed in terms of the masses of the bodies in the system by calculating them directly using the expressions in (3), (4). After expanding D_mA_e , it is easy to see that its trace, being the sum of the diagonal entries is given by

$$\tau = -2k \left(n - 2 + \sum_{q=1}^2 m_q^{-1} \right). \tag{23}$$

Now, to calculate the determinant σ of D_mA_e , we first note that

$$\sigma = |D_mA_e| = |D_m||A_e| \tag{24}$$

$$= \left(\prod_{q=1}^2 m_q^{-1} \right) k^n \left| \frac{1}{k}A_e \right|. \tag{25}$$

Let M_r be the $r \times r$ matrix of the form

$$M_r = \begin{pmatrix} -2 & 1 & & & \\ 1 & -2 & 1 & & \\ & 1 & -2 & 1 & \\ & & \ddots & \ddots & \ddots \\ & & & 1 & -2 & 1 \\ & & & & 1 & -2 \end{pmatrix}, \text{ so that } M_n = \frac{1}{k}A_e.$$

Then, to calculate the determinant $|\frac{1}{k}A_e|$, we use cofactor expansion along the first row to get

$$|\frac{1}{k}A_e| = -2|M_{n-1}| - \begin{vmatrix} 1 & 1 & & & \\ 0 & -2 & 1 & & \\ & 1 & -2 & 1 & \\ & & \ddots & \ddots & \ddots \\ & & & 1 & -2 & 1 \\ & & & & 1 & -2 \end{vmatrix}, \tag{26}$$

where the second term is the determinant of an $n - 1 \times n - 1$ matrix. This term can be simplified by performing cofactor expansion along the first column. This results to

$$|M_n| = -2|M_{n-1}| - |M_{n-2}|, \tag{27}$$

or equivalently

$$|M_n| + 2|M_{n-1}| + |M_{n-2}| = 0, \tag{28}$$

a linear homogeneous recurrence relation with initial conditions $|M_1| = -2$ and $|M_2| = 3$. Since the associated characteristic polynomial of (28) is $x^2 + 2x + 1$, with a double root $x = -1$, the solution is of the form $|M_n| = (c_1 + c_2n)(-1)^n$. Using the initial conditions, we obtain $c_1 = c_2 = 1$ and so $|M_n| = (n + 1)(-1)^n$. Using this in (25), gives

$$\sigma = (n + 1)(-k)^n \prod_{q=1}^2 m_q^{-1}. \tag{29}$$

Let $\tilde{\tau}$ and $\tilde{\sigma}$ be the sum and product of the estimates for the eigenvalues of $D_m A_e$ obtained via the procedure discussed in Sect. 3.2. Then we can relate these data values to the masses of the bodies in the system via the system

$$\begin{cases} \tilde{\tau} = -2k \left(n - 2 + \sum_{q=1}^2 m_q^{-1} \right) \\ \tilde{\sigma} = (n + 1)(-k)^n \prod_{q=1}^2 m_q^{-1} \end{cases}. \tag{30}$$

For the case when $p = 2$, solving the nonlinear system (30) will give the masses of both defects. If $p = 1$, then solving the corresponding equation from the trace relation will be sufficient.

Remark 3.1 The extension of this approach to more defects is mathematically non-trivial. In cases when $p > 2$, one can use other invariants of $D_m A_e$ aside from its trace and determinant, obtained via the Viète relation between the coefficients of the characteristic polynomial and the eigenvalues of $D_m A_e$ on one hand, and the Newton relations between the coefficients of the characteristic polynomial and the traces of $(D_m A_e)^l$, on the other. This approach can be extended iteratively to handle cases when more than two defects are present. In these cases, we need to rely on more matrix invariants to completely determine the defects' masses. The mathematical framework for these cases will be more tedious and will be explored by the authors in a forthcoming article.

Recovering the Locations

In general, once the defects' masses are estimated, the last step is performing an integer optimization to determine the defects' location numbers j_1, j_2, \dots, j_p . This is accomplished by minimizing the L^2 residual function

$$r(j_1, j_2, \dots, j_p) = \int_0^\infty |\tilde{x}_1^*(s, j_1, j_2, \dots, j_p) - \tilde{x}_1(s)|^2 ds. \tag{31}$$

In Eq. (31), \tilde{x}_1^* is taken to be the explicit solution of Eq. (2) in terms of the variable s and the yet unknown parameters j_1, j_2, \dots, j_p .

For the case of two defects located at j_1 and j_2 , we minimize the functional defined in (31) with $p = 2$. In Refs. [8, 9], an analytic solution for \tilde{x}_1^* was given for the case of one and two defects. Let λ satisfy $\cosh \lambda = \frac{s^2 + ds + 2}{2}$ and for $1 \leq i, j \leq n$, define

$$R_{ij} = -\frac{\cosh [(n + 1 - |j - 1|)\lambda] - \cosh [(n + 1 - i - j)\lambda]}{2 \sinh \lambda \sinh [(n + 1)\lambda]}. \tag{32}$$

If there is a single defect on location j with mass m , then

$$\tilde{x}_1^*(s, j) = -\gamma R_{11} - R_{1j}(1 - m)s^2 \cdot \frac{-\gamma R_{j1}}{1 + R_{jj}(1 - m)s^2}. \tag{33}$$

Meanwhile, when there are two defects at locations j_1 and j_2 of masses m_1 and m_2 , respectively, then

$$\begin{aligned} &\tilde{x}_1^*(s, j_1, j_2) \\ &= \frac{-R_{11} + s^2((1 - m_1)R_{1j_1}^2 - (m_2 - 1)R_{1j_2}^2 + (m_1 - 1)R_{11}R_{j_1j_1} + (m_2 - 1)R_{11}R_{j_2j_2})}{1 + s^2((1 - m_1)R_{j_1j_1} + (1 - m_2)R_{j_2j_2} + s^2(m_1 - 1)(m_2 - 1)(R_{j_1j_1}R_{j_2j_2} - R_{j_1j_2}^2))} \\ &+ \frac{s^4(m_1 - 1)(m_2 - 1)(R_{1j_2}^2 R_{j_1j_1} - 2R_{1j_1}R_{1j_2}R_{j_1j_2} + R_{11}R_{j_1j_2}^2 + R_{1j_1}^2 R_{j_2j_2} - R_{11}R_{j_1j_1}R_{j_2j_2})}{1 + s^2((1 - m_1)R_{j_1j_1} + (1 - m_2)R_{j_2j_2} + s^2(m_1 - 1)(m_2 - 1)(R_{j_1j_1}R_{j_2j_2} - R_{j_1j_2}^2))}. \end{aligned} \tag{34}$$

On the other hand, \tilde{x}_1 remains the Laplace transform data obtained from the discrete time measurements. When $q \leq 2$, the minimizer can be found by visually inspecting the plot of r . However, numerical integer optimization techniques will be required for three or more defects.

Numerical Simulations

We will now apply the strategy devised in Sect. 3 to two different 100-body, two-defect spring–mass systems with common parameters given in Table 1. The case of two defects was the selected focus as it is not as simple as a one-defect system but not too computationally complex as a system with three defects. In all cases, the input data, i.e., the longitudinal position of the first body $x_1(t)$ was measured in 50000 t -values with increment $\Delta t = 0.002s$ from 0 to 100 seconds. The simulations for the input data and all intermediate steps taken to fully characterize the defects in each scenario were carried out within MatLab. The first simulation presents a generic scenario where the algorithm worked very accurately. The second and third scenarios involve extreme cases where the accuracy of the method might be limited due to the physical forces in play.

Two Well-Separated Heavy Defects

In this first simulation, we consider the scenario when we have two well-separated defects with relatively high masses. The defect parameters are shown in Table 2.

In lieu of a physical experiment, we shall use simulated data obtained by solving the forward time-domain problem (1) using MatLab’s built-in ODE solver. The solution curve x_1 representing the longitudinal vibration of the first mass as a function of time is shown in Fig. 2.

The Z-transform (as defined in (5)) is applied to the discrete set of time measurements to obtain an estimate for the Laplace domain solution \tilde{x}_1 . Following the discussion in Sect. 3.2, the values of s corresponding to the poles of the estimate for \tilde{x}_1 were computed. This yields our estimates s^2 to the eigenvalues of the system matrix $D_m A_e$. Using these approximate eigenvalues, we obtain the estimates $\tilde{\tau} = -197.3996$ and $\tilde{\sigma} = 10.1822$ for the trace and determinant of the system matrix respectively. Now, Eq. (30) fitted for the parameters of this simulation, reads

$$\begin{cases} \frac{\tilde{\tau}}{2} - 98 = \frac{1}{m_1} + \frac{1}{m_2} \\ \frac{101}{\tilde{\sigma}} = m_1 m_2 \end{cases} \quad (35)$$

Table 1 Common values of system length, defect count, spring constant, impulse scalar, and damping coefficient for the simulations

n	p	k	γ	d
100	2	1	1	0.1

Table 2 Defect parameters for the system in Sect. 4.1

q	1	2
m_q	2	5
j_q	30	60

Solving this 2×2 nonlinear system yields our estimates for the masses, $m_1 = 2.0124$ and $m_2 = 4.9291$, which have relative error of just around 0.62% and 1.42%, respectively.

Lastly, we use the residual function defined in (31), to find the locations j_1 and j_2 of the defects. For cases when there are more than two defects, a numerical optimization routine is necessary to find the integer minimizers of the residual function r . For our case however, we only have two unknowns so we can simply plot r as a function of j_1 and j_2 and observe where the minimum occurs. We use MatLab’s intrinsic integration routine to evaluate r with the integral’s infinite upper bound replaced by 100. This truncation did not affect the quality of the results as both terms in the integrand vanishes rapidly as s increases. The plots in Fig. 3 show different perspectives of the graph of r on a semilogarithmic scale. The top plot shows the 3D graph which suggests the existence of a global minimum. To pinpoint the location numbers, the bottom plots show the projection of the graph to the j_1 - and j_2 -axes. They reveal the minimizers $j_1 = 30$ and $j_2 = 60$, which are indeed the prior unknown locations of the defects.

In this simulation where the defects are relatively heavy and are far apart, the defects were characterized accurately with their masses determined with errors under 2% and their locations computed exactly. This also seems to be the case even if the heavy mass comes first in the chain, as long as there is a moderate separation between the two defects.

The good results we obtained above relied heavily on the use of time-domain data. The choice of using 50,000

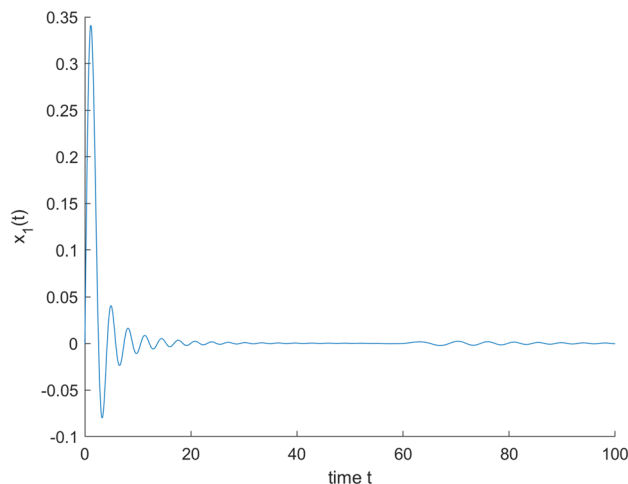
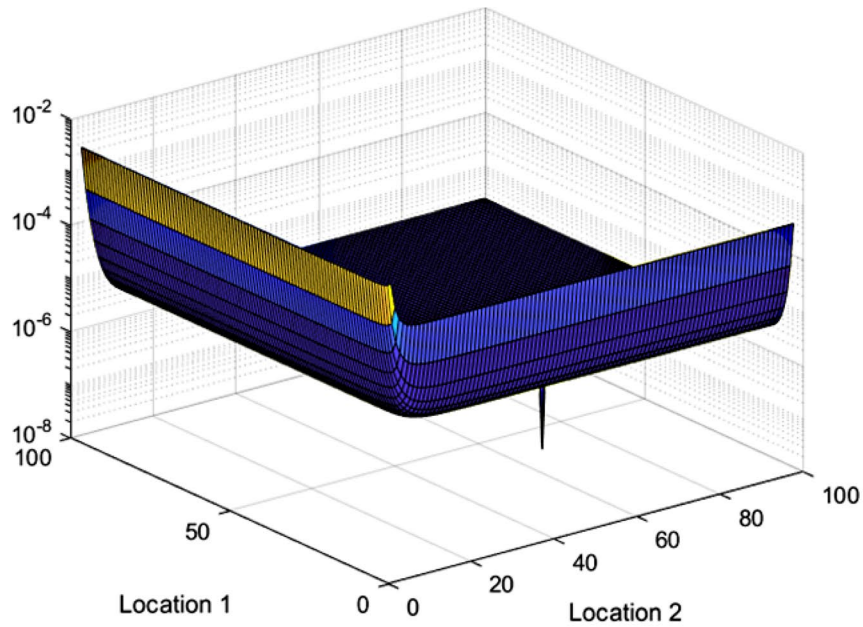


Fig. 2 The solution curve $x_1(t)$ for the spring mass system with defect parameters given in Table 2



(a) Bird's eye view

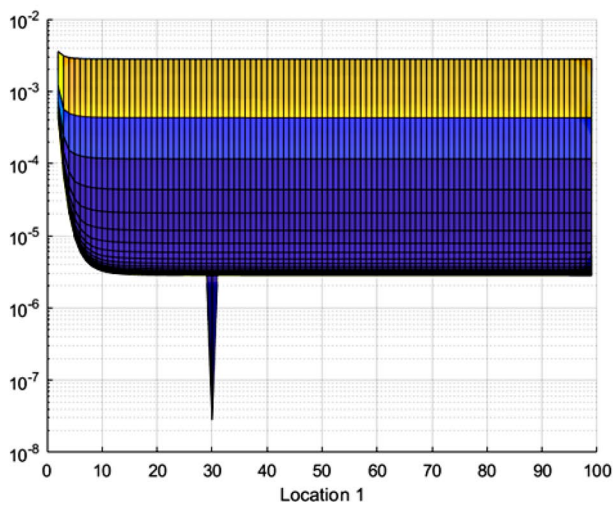
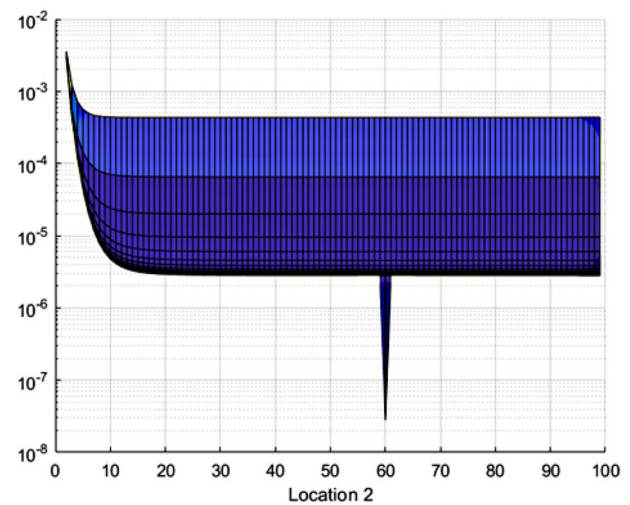
(b) Projection on j_1 axis(c) Projection on j_2 axis

Fig. 3 Plots of the residual as a function of j_1 and j_2 for the spring–mass system of Sect. 4.1

sampling points in time is quite arbitrary and is a result of multiple tests. Theoretically, the more sampling points used, the Z-transform will give better approximation to the Laplace transform. However, performing lots of time domain measurements is impractical in a physical setting. For the spring mass system above, we performed several simulations using different number of time domain points used and recorded the relative errors of the resulting estimates for m_1 and m_2 . The results are shown in Fig. 4.

From this figure, we observe that there are significant errors in both m_1 and m_2 whenever we have less than 35,000 sampling points. Then there is a significant decrease in both errors once we have at least 40,000 sampling points. This suggests that we should use at least 40,000 sampling points in our simulations. A more detailed mathematical and numerical study on the effects of the sampling frequency to the accuracy of the method is warranted to obtain a reliable threshold on the number of measurements required to produce results accurate within desired levels.

Fig. 4 Plot of the relative errors for the estimates to m_1 and m_2 as a function of the number of time-domain measurements used

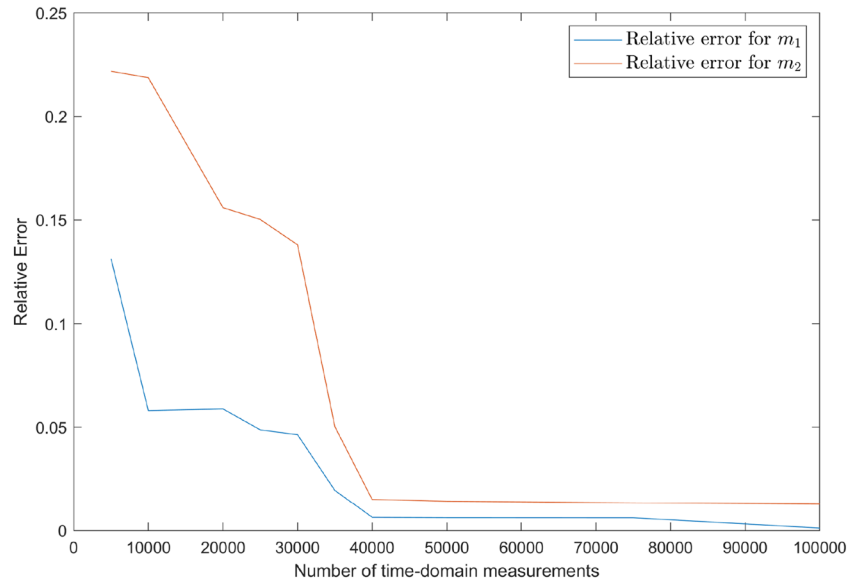


Table 3 Defect parameters for the system in Sect. 4.2

q	1	2
m_q	1.1	3
j_q	49	50

In the next simulations, we test the proposed algorithm in more challenging scenarios when we have two defects that are next to each other.

Two Defects in Close Proximity

Our second simulation will involve the extreme case where we have two defects situated right next to each other near the middle of the chain. In particular, we consider a system with parameters given in Table 3. Note that the first defect has a mass relatively close to the uniform mass in the system.

Again, instead of a physical experiment, we shall use simulated data obtained by solving the forward time-domain problem (1) with the defect parameters given in Table 3 using MatLab’s built-in ODE solver. The solution curve x_1 representing the longitudinal vibration of the first mass as a function of time is shown in Fig. 5. This curve was obtained using 50000 uniformly-spaced points in time with $\Delta t = 0.002$.

Using these 50,000 discrete time measurements in the Z-transform as defined in (6), we obtain an approximation to the Laplace transform \tilde{x}_1 of x_1 . Observing the poles of our approximation to \tilde{x}_1 gives the estimate trace and determinant, $\tilde{\tau} = -198.4844$ and $\tilde{\sigma} = 30.1419$. We then use these values in our matrix invariants relations:

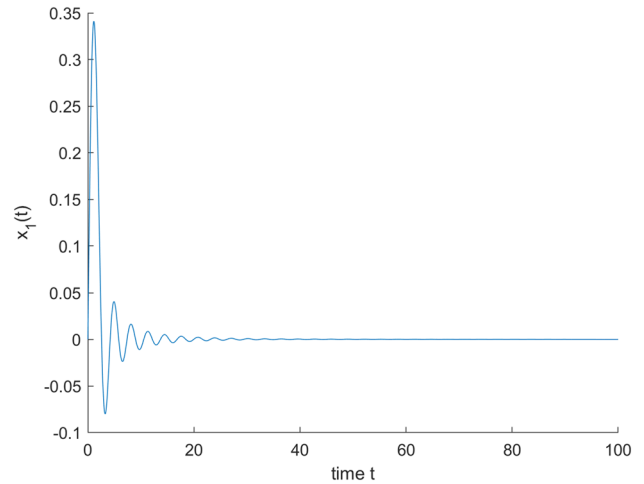
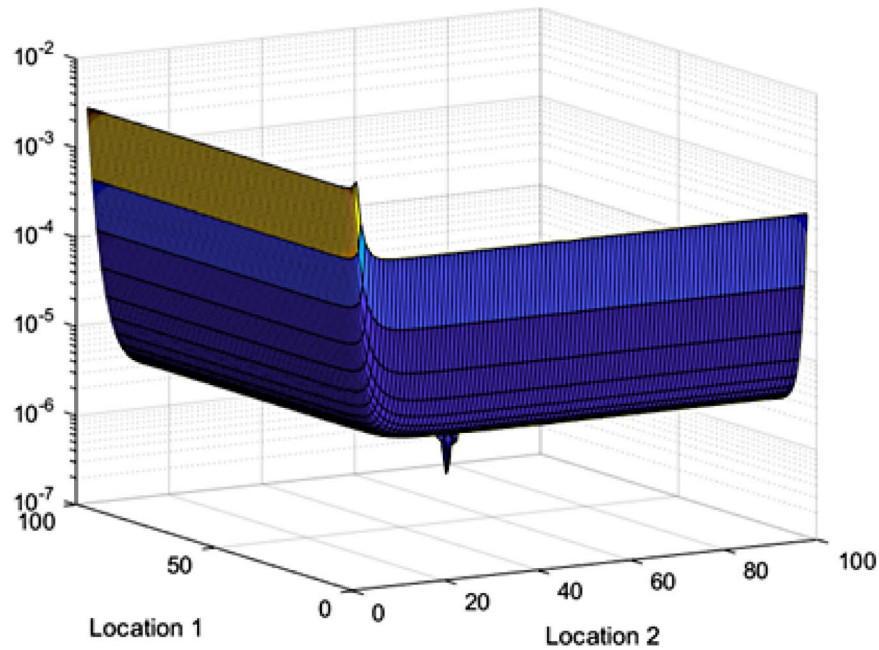


Fig. 5 The solution curve $x_1(t)$ for the spring mass system with defect parameters given in Table 3

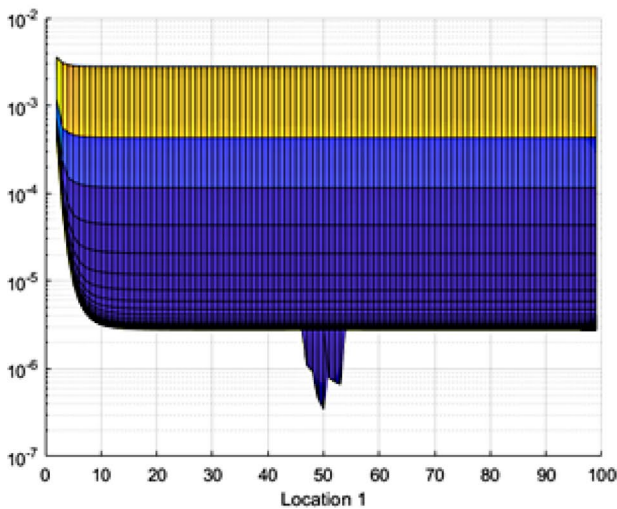
$$\begin{cases} \frac{\tilde{\tau}}{2} - 98 &= \frac{1}{m_1} + \frac{1}{m_2} \\ \frac{101}{\tilde{\sigma}} &= m_1 m_2 \end{cases} \quad (36)$$

Solving this nonlinear system results to $m_1 = 1.0910$ and $m_2 = 3.0714$, which have relative errors of just around 0.82% and 2.38%, respectively.

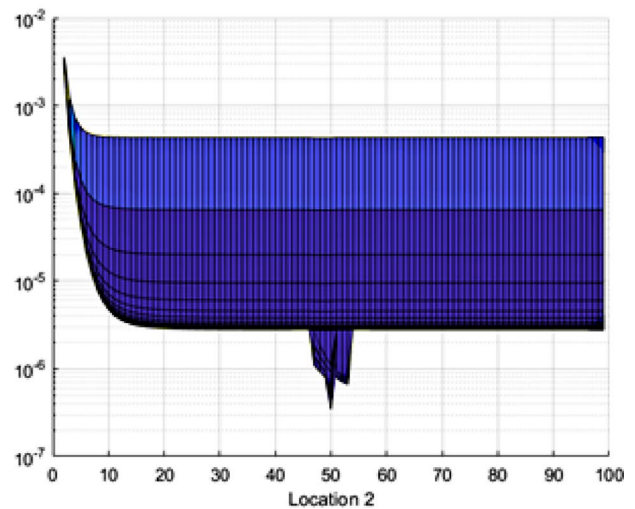
Now, we try to obtain the locations of the defects by plotting the residual function (of the defect locations j_1 and j_2) as defined in (31). Figure 6 offers three views of the graph of the residual function. The minimum of r occurs at $j_1 = j_2 = 50$. This indicates that the algorithm’s best ‘guess’ is that there is only one defect located at position



(a) Bird's eye view



(b) Projection on j_1 axis



(c) Projection on j_2 axis

Fig. 6 Plots of the residual as a function of j_1 and j_2 for the spring–mass system of Sect. 4.2

50. This ‘anomaly’ makes sense from a physical point of view as the defect at position 50 is three times heavier than all non-defective bodies while the defect at position 49 has actual mass 1.1, which is close to the uniform mass. This ‘tricks’ our algorithm into thinking that the two defects are just a very heavy single defect. In cases like this, when the minimizer of the residual is the point of the form (j, j) , but one is sure that there are two defects, we can look at the point with the second smallest residual (which in most of the times will be the point of the form $(j_1 \pm 1, j_2)$ or

Table 4 Defect parameters for the system in Sect. 4.3

q	1	2
m_q	3.1	3
j_q	49	50

$(j_1, j_2 \pm 1)$. In our simulation, the second smallest residual occur at $(49, 50)$ which gives the exact locations of the defects. For reference, $r(50, 50) \approx 3.4496 \times 10^{-7}$ while $r(49, 50) \approx 4.6656 \times 10^{-7}$.

Two Defects of Almost the Same Mass in Close Proximity

In this simulation, we subject our proposed scheme to a more difficult scenario where we have two defects of almost the same size that are next to each other. Specifically, we still consider a 100-mass system with unknown defect parameters given in Table 4. Here we see that unlike the previous simulation, the masses of the defects are relative close to each other, with relative difference of just about 3.33%.

As in the previous cases, we shall use simulated data instead of physical time-measurements. These are obtained using Matlab’s intrinsic ODE solver over the time interval [0, 100] with time increment $\Delta t = 0.002$. The solution curve showing the displacement $x_1(t)$ of the left-most body at a give time t is shown in Fig. 7.

Using these 50000 data points, we approximated the Laplace transform \tilde{x}_1 of the time-domain curve x_1 using the Z-transform defined in (6). Then following the discussions in Sects. 3.2 and 3.3, we used the approximate poles of \tilde{x}_1 to obtain some estimates to the eigenvalues of the system matrix $D_m A_e$. This resulted to our estimates for the system matrix’ trace and determinants: $\tilde{\tau} = -197.311830$ and $\tilde{\sigma} = 10.863558$, respectively. These values give rise to the following system of equations that will yield our estimates for the unknown masses m_1 and m_2 :

$$\begin{cases} \frac{\tilde{\tau}}{2} - 98 = \frac{1}{m_1} + \frac{1}{m_2} \\ \frac{101}{\tilde{\sigma}} = m_1 m_2 \end{cases} \quad (37)$$

Solving this system gives our estimates for the masses: $m_1 \approx 3.049267$ and $m_2 \approx 3.049267$, with relative errors of about 1.745362×10^{-2} and 1.745069×10^{-2} , respectively. We see that the algorithm was still able to produce accurate

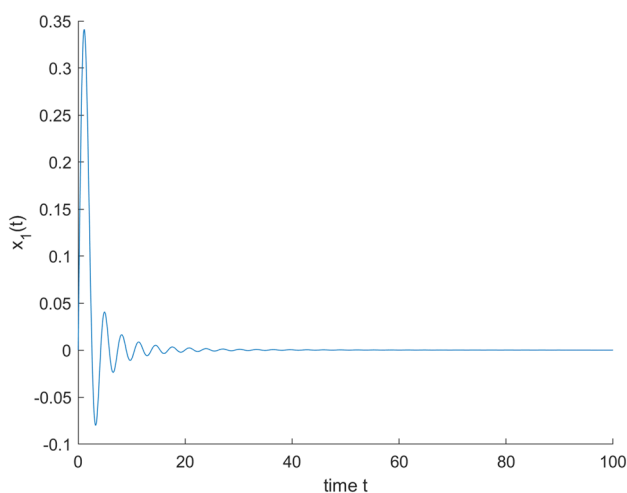


Fig. 7 The solution curve $x_1(t)$ for the spring mass system with defect parameters given in Table 4

estimates for the masses. Now, to predict the locations of the defects, we plot the residual function (of the defect locations j_1 and j_2) as defined in (31) and see where its minimum occurs. The graph is given in three perspectives in Fig. 8.

The plot shows that indeed the residual is minimized near the middle of the chain. The minimum value $r(j_1, j_2)$ occurs at the point (49, 50) with $r(49, 50) \approx 3.6609 \times 10^{-7}$. This shows that the algorithm predicted the locations exactly. However, on a close second is the value $r(50, 49) \approx 3.8909 \times 10^{-7}$. This indicates that it is likely that the algorithm will interchange the locations of these two defects, which is understandable since the two defects have very similar masses and they are on very close proximity.

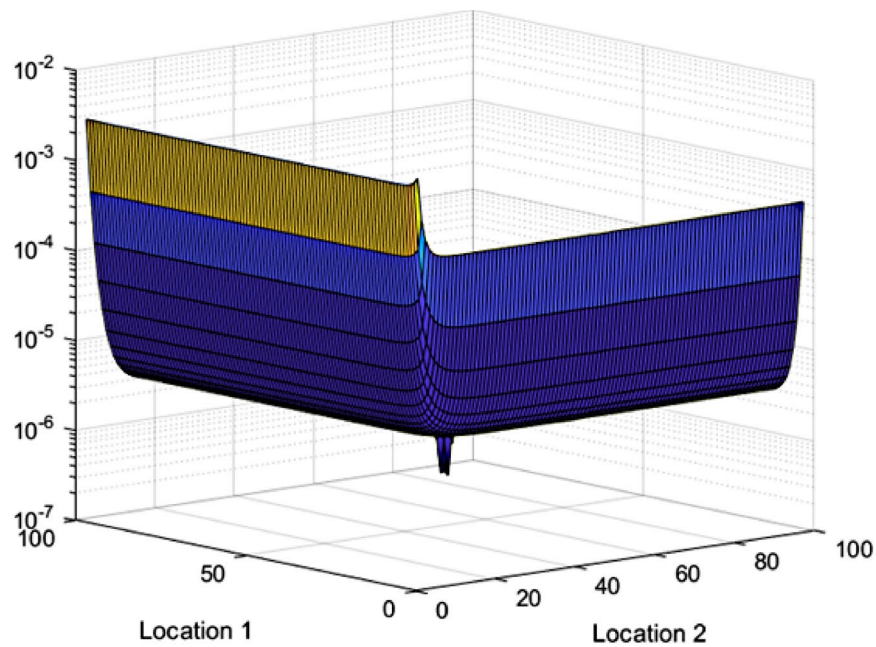
Remark 4.1 Our numerical investigations suggest that this method is stable with respect to measurement noise. We performed numerical tests in which the time-domain measurements were perturbed by 1% Gaussian noise. In these simulations, the defects’ masses were predicted with error of just at most 5% while the defects’ locations where retrieved accurately.

Conclusion

In summary, we devised and executed an algorithm determining the location and masses of defects embedded within a 1D spring–mass system of known length. Particularly, the characteristics of the defects were recovered using solely some discrete measurements of the vibrations of the first body in the chain.

Assuming a sufficiently small spring damping coefficient, the algorithm developed consists of four steps: (1) gathering discrete time-domain data and converting it into the Laplace domain data \tilde{x}_1 via the Z-transform, (2) obtaining estimates for the system’s eigenvalues using the poles of \tilde{x}_1 on the complex plane, (3) recovering the masses of the defects by solving a non-linear system of equations involving the system’s trace and determinant, and (4) determining the locations of each defect by minimizing an L^2 residual function.

This algorithm was applied to three independent spring–mass systems with two defects. The first involves a generic case of having two defects with moderate to generous separation. In this case, very accurate results for both the masses and locations of the defects were obtained. The second simulation presented some of the limitations of the algorithm, in which the physical configuration of the system led to difficulties of characterizing all the parameters of the defects with high accuracy. The algorithm thought that there is only one huge defect at the location of the bigger defect. However, since we know that there are two defects in the chain, we look at minimum residual value $r(i, j)$ where $i \neq j$. The last simulation involves two similar



(a) Bird's eye view

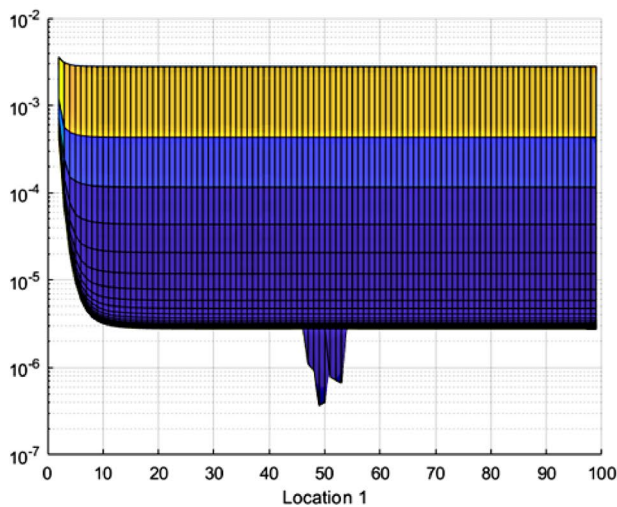
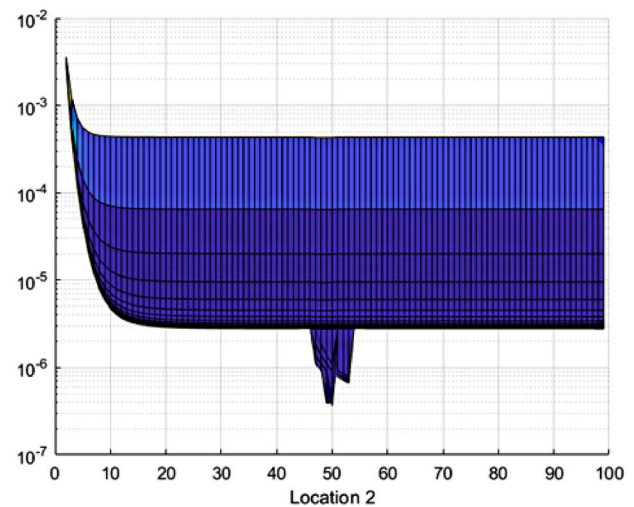
(b) Projection on j_1 axis(c) Projection on j_2 axis

Fig. 8 Plots of the residual as a function of j_1 and j_2 for the spring–mass system of Sect. 4.3

defects next to each other. The defects' masses were estimated accurately but the determination of the locations is a bit of a challenge. This is attributed to the fact that the masses of the two defects are relatively near to each other.

The proposed scheme, in the current form applied in the simulations above, though backed by a very general mathematical framework, has some limitations. First, the scheme illustrated only works for cases with one or two defects. An adaptation and extension of parts of the mathematical framework (described below) is needed to

accommodate the case of an arbitrary number of defects and unknown defect parameters. Second, some accuracy in the determination of the unknown masses is lost when the defects are next to each other. This is a physical limit as the two proximal defects may be seen as a single larger defect, especially for longer systems. Lastly, the scheme only works well when the damping coefficient is small enough. This was required by the asymptotics used in the mathematical framework. This can be remedied through the use of exact expressions in the manipulation of Eq. (8),

but at a very high computational expense that is impractical, especially for systems with more than ten bodies.

The authors plan to perform some numerical investigations for cases when there are more than two defects. We already alluded to the theoretical framework that can be used in determining the masses of the defects, i.e., via the Viète relations for the characteristic polynomial and the eigenvalues of $D_m A_e$ and the Newton relations for the characteristic polynomial and the traces of $(D_m A_e)^l$. Obtaining the location of the defects will also be more computationally involved as simply plotting r will not work. For this, we shall need numerical integer optimization techniques.

An interesting follow-up to this work would be the application of the algorithm in a physical setting where we do actual measurements of the vibrations in the first mass. One can also extend this work and explore the possibility of using measurements from both ends of the chain to address the limitations of the current work. We can also do a numerical study by performing sensitivity tests with respect to the damping coefficient. Our current method assumes a small damping coefficient d , so it might be worthwhile to look at the effects of the magnitude of d on the quality of results and perhaps find an acceptable threshold or upperbound for it. Another immediate extension would be to study the case of non-negligible damping coefficient. We also mentioned above the reliance of the method on discrete time measurements. Hence, a mathematical and numerical study on the effects of sampling frequency on the accuracy of the results is worthwhile. This may lead us to determining a threshold on the number of time-domain measurements required so that the results are within some error bounds. Further extensions to the work presented here include, but are not limited to: non-Hookean spring–mass systems, scenarios where every spring has a different stiffness/damping property, and multi-dimensional spring–mass arrays.

Funding Larry Guan was supported by the University of Houston through an Undergraduate Research Fellowship.

Availability of data and material Not applicable.

Code availability Not applicable.

Declarations

Conflict of interest The authors do not have conflicts of interest or competing interests.

References

- Akulenko LD, Nesterov SV (2014) Mass defect influence on the longitudinal vibration frequencies and mode shapes of a beam. *Mech Solids* 49:104–111
- Bae J-S, Hwang J-H, Kwag D-G, Park J, Inman DJ (2014) Vibration suppression of a large beam structure using tuned mass damper and eddy current damping. *Shock Vib* 1–10:2014
- Caniato M, Bettarello F, Marsich L, Ferluga A, Sbaizero O, Schmid C (2016) Impulse response method for defect detection in polymers: description of the method and preliminary results. *Polym Test* 55:78–87
- Clark W (2000) Vibration control with state-switched piezoelectric materials. *J Intell Mater Syst Struct* 11(4):263–271
- Corr L, Clark W (2003) A novel semi-active multi-modal vibration control law for a piezoceramic actuator. *J Vib Acoust* 125(2):214–222
- Deymier P, Runge K (2016) One-dimensional mass-spring chains supporting elastic waves with non-conventional topology. *Crystals* 6(4):44
- Dove MT (2011) Introduction to the theory of lattice dynamics. *JDN* 12:123–159
- Egarguin NJA, Meklachi T, Onofrei D, Harari-Arnold ND (2020) Correction to: Vibration suppression and defect detection schemes in 1D linear spring-mass systems. *J Vib Eng Technol* 8:621
- Egarguin NJA, Meklachi T, Onofrei D, Harari-Arnold ND (2020) Vibration suppression and defect detection schemes in 1d linear spring-mass systems. *J Vib Eng Technol* 8:489–503
- El Saif M, Foda MA (2001) Vibration suppression of a beam structure of intermediate masses and springs. *J Sound Vib* 256(4):629–645
- Faleski Michael C (2006) Transient behavior of the driven lc circuit. *Am J Phys* 74(5):429–437
- Getachew G (2018) A review of simple harmonic motion for mass spring system and its analogy to the oscillations in lc circuit. *J Phys Chem Sci* 6(3)
- He ZC, Xiao X, Li E (2017) Design for structural vibration suppression in laminate acoustic metamaterials. *Compos Part B Eng* 131:237–252
- Horn RA, Johnson CR (2013) Matrix analysis, 2nd edn. Cambridge University Press, Cambridge
- Jarrousse O (2012) Modified mass–spring system for physically based deformation modeling. Ph.D. thesis
- Joannopoulos JD, Johnson SG, Winn JN, Meade RD (2008) Photonic crystals: molding the flow of light, 2nd edn. Princeton University Press, Princeton
- Li T, Li Q, Liu T (2019) An actuated dissipative spring-mass walking model: predicting human-like ground reaction forces and the effects of model parameters. *J Biomech* 90:58–64
- Liu T, Bargteil AW, O'Brien JF, Kavan L (2013) Fast simulation of mass–spring systems. *ACM Trans Gr* 32(6):1–7
- Martin WC, Wu A, Geyer H (2015) Robust spring mass model running for a physical bipedal robot. In: 2015 IEEE international conference on robotics and automation (ICRA), Seattle, WA, USA, pp 6307–6312
- Minaya R, Ponce Y (2017) Applications of spring–mass model on crystalline lattices. 09
- Morgan D, Qiao S (2008) Accuracy and stability in mass-spring systems for sound synthesis. In: Proceedings of C3S2E-08, pp 1–12
- Nealan A, Muler M, Keiser R, Boxerman E, Carlson M (2005) Physically based deformable models in computer graphics. *Comput Gr Forum* 25(4):809–836
- Nedel L, Thalmann D (1998) Real time muscle deformations using mass-spring systems. In: Proceedings of the computer graphics international, pp 157–177
- Patel VN, Tandon N, Pandey RK (2012) Defect detection in deep groove ball bearing in presence of external vibration using envelope analysis and duffing oscillator. *Measurement* 45(5):960–970

25. Peng H, Frank Pai P (2014) Acoustic metamaterial plates for elastic wave absorption and structural vibration suppression. *Int J Mech Sci* 89:350–361
26. André Preumont (2011) *Vibration control of active structures, an introduction*. Solid mechanics and its applications, 3rd edn. Springer, Berlin
27. Qin Y, Xiang C, Wang Z, Dong M (2017) Road excitation classification for semi-active suspension system based on system response. *J Vib Control* 24(13):2732–2748
28. Radetzky A, Nurnberger A, Teistler M, Pretschner DP (1999) Elastodynamic shape modeling in virtual medicine. In: *Proceedings shape modeling international '99*. International conference on shape modeling and applications, Aizuwakamatsu, Japan, pp 172–178
29. Taylor MJD, Beneke R (2012) Spring mass characteristics of the fastest men on earth. *Int J Sports Med* 33:667–670
30. Wang HP, Mustafa GIY, Tian Y (2018) Model-free fractional-order sliding mode control for an active vehicle suspension system. *Adv Eng Softw* 115:452–461
31. Yang J, Shang S (2013) Cloth modeling simulation based on mass spring model. *Appl Mech Mater* 310:676–683
32. Yao S, Zhou X, Hu G (2008) Experimental study on negative mass effective mass in a 1d mass-spring system. *New J Phys* 10(4):1–4
33. Zerbato D, Galvan S, Fiorini P (2007) Calibration of mass spring models for organ simulations. In: *2007 IEEE/RSJ international conference on intelligent robots and systems*, San Diego, CA, USA, pp 370–375
34. Zhang S, Gu L, Huang P, Xu J (2005) Real-time simulation of deformable soft tissue based on mass-spring and medial representation. In: *Computer vision for biomedical image applications, a workshop of ICCV2005*, LNCS 3875, pp 419–426
35. Zhenfang C, Bing H (2012) Research of fast cloth simulation based on mass-spring model. In: *National conference on information technology and computer science (CITCS 2012)*, Lanzhou, China

Publisher's Note Springer Nature remains neutral with regard to jurisdictional claims in published maps and institutional affiliations.